Earth and Planetary Science Letters 302 (2011) 27–37

Contents lists available at ScienceDirect

Earth and Planetary Science Letters

journal homepage: www.elsevier.com/locate/epsl

Continental collision and slab break-off: A comparison of 3-D numerical models with observations

Jeroen van Hunen *, Mark B. Allen

Department of Earth Sciences, University of Durham, Durham DH1 3LE, United Kingdom

ARTICLE INFO

Article history:
Received 8 September 2010
Received in revised form 14 November 2010
Accepted 18 November 2010
Available online 24 December 2010

Editor: P. Sheare

Keywords:
subduction
continental collision
slab break-off
slab detachment
numerical modelling
Arabia–Eurasia

ABSTRACT

Conditions and dynamics of subduction–collision and subsequent 3-D slab break-off and slab tear propagation are quantified, for the first time, using fully dynamic numerical models. Model results indicate that collision after the subduction of old, strong subducting oceanic slab leads to slab break-off at 20–25 Myr after the onset of continental collision, and subsequently a slab tear migrates more or less horizontally through the slab with a propagation speed of 100–150 mm/yr. In contrast, young, weak oceanic slabs show the first break-off already 10 Myr after continental collision, and can experience tear migration rates up to 800 mm/yr. Slab strength plays a more important role in the timing of slab break-off and the speed of a propagating slab tear than (negative) slab buoyancy does. Slab break-off is viable even for slabs that are supported by the viscosity jump and phase change between the upper and lower mantle.

The density of the oceanic slab and the subducting continental block is important for the amount of continental subduction and the depth of slab break-off. A 40-km thick continental crust can be buried to depths greater than 200 km, although this maximum depth is significantly less for younger or very weak slabs, or thicker continental crust. Slab break-off typically starts at a depth of 300 km, mostly independent of mantle rheology, but, like continental crustal burial, can be shallower for young or buoyant plates. Our 3-D models illustrate how, due to the difference in necking in 2-D and 3-D, break-off has an intrinsic small preference to start as a slab window within the slab's interior, rather than as a slab tear at the slab edge. However, any significant asymmetry in the collision setting, e.g. earlier collision at one end of the subduction zone, would override this, and leads to slab tearing starting near one edge of the slab.

These results put important new constraints on the dynamics of the collision and subsequent slab break-off for modern collision belts. For a proposed timing of the initial Arabia–Eurasia collision at 35 Ma, break-off of the ~200-Myr-old Neo-Tethys slab is unlikely to have occurred before 15–10 Ma. Furthermore, our results illustrate that shallow, early break-off of weak slabs provides a viable explanation for the absence of blueschists and ultra-high pressure metamorphism in the Precambrian geological record.

1. Introduction

Continental collision is a natural consequence of plate tectonics and continental drift, where closure of an oceanic basin leads to onset of subduction of buoyant continental material. This will slow down and eventually stop the local subduction process. Collision of Arabia with Eurasia and India with Eurasia has produced mountain ranges and plateaux across much of present-day SW and Central Asia.

In such a continental collision scenario, the buoyant continental lithosphere at the surface is connected to the previously subducted oceanic lithosphere. This leads to tensile stresses between the two lithospheres that lead to the separation of the oceanic slab from the continental lithosphere at the surface (e.g., Davies and von Blanckenburg, 1995; Wortel and Spakman, 1992). How this separation occurs is unclear. Perhaps, the slab slowly thermally dissolves, and is gradually 'absorbed' in the mantle. Or perhaps separation is rapid, vigorous, and localized, when the slab breaks away from the continent above, and sinks into the mantle. The latter is commonly referred to as slab break-off or slab detachment. Theoretical studies (Davies and von Blanckenburg, 1995; Yoshioka and Wortel, 1995) illustrate the occurrence of slab break-off, and recent dynamical modelling work (Andrews and Billen, 2009; Gerya et al., 2004) suggests initial necking of the slab, until it is mechanically disconnected from the continent above and can sink down.

Many previous studies have discussed the conceptual model of slab break-off using a range of observations. Early work by Isacks and Molnar (1969) speculated on the occurrence of slab break-off as a possible explanation of gaps in the earthquake distributions. Post-collisional magmatism has been attributed to slab break-off, where the detachment of the slab from the lithosphere above would leave a slab window, through which hot mantle material is put in direct contact with the overriding plate or the hydrated mantle wedge (Davies and von Blanckenburg, 1995; Ferrari, 2004; van de Zedde and Wortel, 2001;

* Corresponding author. Tel.: +44 191 3342293.
E-mail address: jeroen.van-hunen@durham.ac.uk (J. van Hunen).

0012-821X/$ – see front matter © 2010 Elsevier B.V. All rights reserved.
doi:10.1016/j.epsl.2010.11.035

Wong-A-Ton and Wortel, 1997). This process has been linked to magmatism in the Alps (Davies and von Blanckenburg, 1995), Turkish–Iranian plateau (e.g., Dargahi et al., 2010; Keskin, 2003; Omrani et al., 2008), Central America (Ferrari, 2004), and the Appalachians (Whalen et al., 2006).

High resolution seismic tomography provides a powerful tool to image subducted slabs. This technique has been applied to illustrate the presence of gaps in subducted slabs. These seismically detected slab windows could be associated with partly or fully detached lithosphere in the Mediterranean (Carminati et al., 1998; Wortel and Spakman, 2000); Carpathians (Wortel and Spakman, 2000; but see Lorinczi and Houseman, 2009) and Turkish–Iranian plateau (Hafkenscheid et al., 2006).

Surface expressions of slab break-off have been suggested, both on the basis of observations and numerical model calculations. Uplift on the order of 100 s of metres to several kms after slab break-off has been reported for the Apennines (e.g., van der Meulen et al., 1999; Westaway, 1993). Elasto-plastic models of subduction–collision and break-off (Buiter et al., 2002) and visco-plastic models of break-off after collision (Andrews and Billen, 2009; Gerya et al., 2004) illustrate significant uplift (1–10 km) and uplift rates (0.1–2.5 km/Myr) associated with slab break-off. This range of reported uplift from both observations and models illustrates the complexity of this process, and more work is required before surface uplift will prove a valuable diagnostic of slab break-off. Of particular importance is the ability to distinguish uplift by slab break-off from uplift due to changes in the subduction process (Buiter et al., 2002) or lithospheric delamination processes (Gogus and Pysklywec, 2008; Lorinczi and Houseman, 2009).

Although slab break-off has been suggested to occur during the subduction of very young plates or mid-ocean ridges (e.g. for Central America, Burkett and Billen, 2009; Ferrari, 2004; Rogers et al., 2002), or locally even for the subduction of mature oceanic lithosphere (Levin et al., 2002), this study focuses on the scenario of continental collision. For collisional settings, several dynamic modelling studies illustrate that break-off does not occur immediately at collision, but typically takes 5–30 Myrs to complete (Andrews and Billen, 2009; Gerya et al., 2004). In addition, continental collision is not a geologically instantaneous process (Royden, 1993), and the transition from subduction to collision may have an important influence on the timing of break-off. Slab break-off is often invoked to explain post-collisional magmatism, and even for one region the interpreted timing of break-off varies significantly between studies. E.g., for the Turkish–Iranian plateau, slab detachment has been proposed for a range of geological times, from 40 to 5 Ma (e.g., Ghasemi and Talbot, 2006; Omrani et al., 2008). A good understanding of the relative timing of continental collision and slab break-off will provide useful constraints on the dynamics of continental collision.

Unlike generic subduction, slab break-off is intrinsically a 3-D process. Reconstruction of the closure of the Neo-Tethys ocean illustrates that continental collision typically occurs at 100 s–1000 s km segments of the subduction zone, while outside the segments, oceanic subduction continues (e.g., Hafkenscheid et al., 2006). In addition, slab break-off itself is unlikely to occur in a 2-D trench-perpendicular fashion. Instead, observations from tomography (e.g., Wortel and Spakman, 2000), magmatism (Omrani et al., 2008), and depocentre migration (Meulenkamp et al., 1996) indicate that slab break-off is expected to occur by a laterally propagating tear in the slab. Theoretical models suggest a wide range of possible tear migration rates (Yoshioka and Wortel, 1995), and illustrate the importance of dynamical aspects such as slab rheology, plate coupling, and convergence rate. Fully 3-D dynamical, time-dependent models are required to link continental collision and tear migration to the proposed observables.

Slab break-off is driven by the extensional stresses created by the combined positive buoyancy of the subducting continental lithosphere and the negative buoyancy of the previously subducted slab. In that context, the supporting role of the endothermic spinel-to-perovskite phase transition might play an important role. Combined effects for this phase transition of resistance against sinking of cold material and a 10–100-fold increase in viscosity can locally lead to slabs stagnating in the transition zone, as illustrated from seismic tomography (van der Hilst et al., 1991). For several regions where slab break-off is proposed (e.g. the Mediterranean, Wortel and Spakman, 2000), slabs seem to stagnate (at least temporarily) at the base of the upper mantle. Such local support of slabs would reduce the extensional stresses within those slabs, and could alter or prohibit slab break-off. Many previous modelling studies on slab break-off have examined the break-off of short slabs that freely hang in the upper mantle, without significant support from the base of the mantle. Whether and how slabs break off if they are supported in the transition zone is still uncertain.

In this paper, we present the first 3-D, fully dynamic models of continental subduction and subsequent slab break-off. We show how break-off evolves in three dimensions, how this differs from a 2-D scenario, and how break-off applies to slabs that are supported in the transition zone. We systematically investigate effects of plate age and strength, characteristics of the subducting continent, and mantle rheology. By producing observables such as delay times between collision and break-off and depth of continental crust burial and slab break-off, we provide a means to make direct quantitative comparisons between model results and observations. We finally discuss applications of these results, and illustrate their relevance to both modern collision sites, such as the Arabia–Eurasia collision, and continental collision in the Precambrian.

2. Model description

2.1. Model setup

Closure of a small oceanic basin, and subsequent continental collision and slab break-off are modelled in a vertical 2-D or full 3-D rectangular domain (Fig. 1). A subducting oceanic lithosphere with a continental block embedded within is positioned next to a fully continental overriding lithosphere. The computational domain is 660 km deep (slabs are assumed to stagnate at the base of the upper mantle), and has an aspect ratio of 1:4 (in 2-D) and 1:4:4 (in 3-D). These and other model parameters are presented in Table 1.

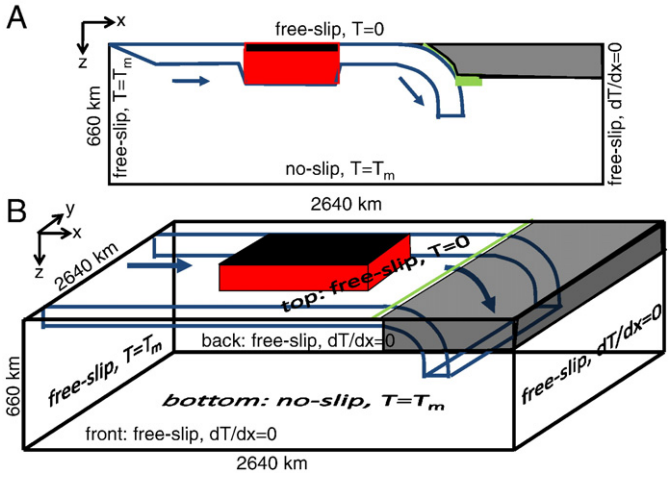

Fig. 1. Model setup in A) 2-D, and B) 3-D, including dimensions and mechanical and thermal boundary conditions. The model extends to 660 km depth and has a 1:4 or 1:4:4 aspect ratio. The subducting plate (schematically outlined in blue) has a continental block (embedded (red) with a buoyant continental crust (black). Subducting and overriding plates are decoupled by a weak zone and a weak mantle wedge (green). In 3-D, the subducting plate is decoupled from the platelets at the front and back of the model domain by a transform fault. Blue arrows indicate the subducting plate motion.

The resistance of the continental block to subduction is realized through the compositional buoyancy of continental crust. Near the surface, the much thinner basaltic oceanic crust would be buoyant too. But, unlike the dry and/or granitic continental crust, hydrated basaltic oceanic crust is expected to transform into eclogite below 30–40 km, where it has a density comparable to mantle material. Therefore, the net effect of oceanic crustal buoyancy will be relatively small (Cloos, 1993; Korenaga, 2006). To avoid the model becoming overly complicated, we model the continental crust with a uniform compositional buoyancy, and omit the much smaller buoyancy effect of the oceanic crust.

Initially, the continental block and overriding continental lithosphere both have a linear temperature from 0 °C at the surface to mantle temperature at maximum plate depth (150 km in the default model). Temperature variation arising from radiogenic heat production (e.g. in the continental crust) is negligible given the short time span of the model calculations. Oceanic lithosphere follows the cooling half-space solution for a given plate age (Turcotte and Schubert, 2002). At the start of the model, this plate age increases linearly from 0 Myrs at the mid-ocean ridge on the left corner of the model domain to a given subduction age at and beyond the trench (van Hunen et al., 2002). A slab initially extends down halfway into the upper mantle. This is a convenient and often applied geometry that provides enough slab pull to drive subduction without external forcing, and allows the complex slab–transition zone interaction to be dealt with self-consistently. An associated drawback is initial subduction without much mantle drag resistance, which results in an artificial, high initial peak subduction velocity (see Fig. 3). We varied the plate age at the trench between 35 and 90 Myr. Bathymetry and surface heat flow observations show that older oceanic plates follow a plate model (Parsons and Sclater, 1977; Stein and Stein, 1992), possibly due to small-scale lithospheric instabilities (Parsons and McKenzie, 1978; van Hunen et al., 2005), and are therefore expected to behave mechanically similar to the 90-Myr-old plate. A uniform mantle temperature of the underlying mantle is in line with the adopted Boussinesq approximations. Note that subduction ages for later model times may deviate somewhat from the initially imposed plate age, since the subduction velocity is not imposed, but is freely developing in each calculation. The following thermal boundary conditions apply (see also Fig. 1). The left (i.e. $x=0$) boundary and the bottom boundary have a fixed mantle temperature $T_m=1350$ °C. The surface has a uniform temperature of 0 °C, and the right boundary (i.e. $x=2640$ km) is modelled as a symmetry boundary (i.e. zero heat conduction through that boundary). As mechanical boundary conditions, all boundaries are closed to flow. The flow field has free-slip conditions on all boundaries except the bottom boundary, where a no-slip condition applies to model the effect of the much higher-viscosity lower mantle (Gurnis and Hager, 1988).

Table 1
Symbols, units and default model parameters used in this study.

Symbol	Description	Default value and units
A	Rheological pre-exponent	10^{20} (df), 2.8×10^{13} (ds) [$Pa^{-n}\,s^{-1}$]
E^*	Activation energy	360 [kJ/mol]
e_z	Vertical unit vector	[–]
g	Gravitational acceleration	9.8 [m/s^2]
h	Model height	660 [km]
n	Rheological power law exponent	1 (df), 3.5 (ds) [–]
P	Deviatoric pressure	[Pa]
p_0	Lithostatic pressure	[Pa]
R	Gas constant	8.3 [J/mol]
Ra	Thermal Rayleigh number	4.4×10^6 [–]
Rb	Compositional Rayleigh number	1.7×10^7 [–]
T	Temperature	[°C]
T_{abs}	Absolute temperature	[K]
T_m	Mantle temperature	1350 [°C]
t	Time	[s]
u	Velocity	[m/s]
α	Thermal expansion coefficient	3.5×10^{-5} [K^{-1}]
ΔT	Temperature drop over model domain	1350 [K]
$\dot{\varepsilon}$	Strain rate	[s^{-1}]
η	Viscosity	[Pa s]
η_0	Reference viscosity	10^{20} [Pa s]
μ	Friction coefficient	0.1 [–]
κ	Thermal diffusivity	10^{-6} [m^2/s]
ρ	Density	[kg m^{-3}]
σ	Stress	[Pa]
τ_y	Yield stress	[MPa]
τ_0	Surface yield stress	40 [MPa]
τ_{max}	Maximum yield stress	400 [MPa]

2.2. Rheology

The strength of the lithosphere is governed through temperature-dependent viscous deformation of both diffusion creep (with effective viscosity η_{diff}) and dislocation creep (with effective viscosity η_{disl}) (Hirth and Kohlstedt, 2003; Karato and Wu, 1993; Korenaga and Karato, 2008). Both η_{diff} and η_{disl} are described by the following viscosity description:

$$\eta = A\dot{\varepsilon}^{\frac{1-n}{n}}\exp\left(\frac{E^*}{nRT_{abs}}\right) \quad (1)$$

with $\dot{\varepsilon}$ the second invariant of the strain rate, E^* the activation energy, n the power–law exponent (from dry dislocation creep from Karato and Wu, 1993), T the absolute temperature, and A a pre-exponential constant. Zero activation volume is assumed here to keep the model simple and in line with ignoring the effects of adiabatic compression in the Boussinesq approximation. In addition, close to the surface brittle yielding of material reduces the strength (Byerlee, 1978; Kohlstedt et al., 1995), and mantle material will yield under higher lithostatic pressure by stress-limiting mechanisms such as Peierls' creep mechanism (Kameyama et al., 1999). We combine these two yielding mechanisms into a simplified stress-limiting rheology, for which the viscosity is described as:

$$\eta = \frac{\tau_y}{2\dot{\varepsilon}} \quad (2)$$

with the yield stress τ_y described as:

$$\tau_y = \min(\tau_0 + \mu p_0, \tau_{\max}) \quad (3)$$

where τ_0 is the yield stress at the surface, p_0 is the lithostatic pressure, μ is the friction coefficient (Byerlee, 1978), and τ_{max} is the maximum yield stress. The effective viscosity η_{eff} is simply defined as the minimum of the individual viscosity components. This is somewhat different from the slightly more complex composite rheology in which the harmonic mean rather than the minimum of the diffusion and dislocation creep strengths are used (van den Berg et al., 1993). Upper mantle values for A are based on the observations that a) the effective viscosity of the shallow upper mantle is on the order of 10^{20} Pa s (e.g., Hager, 1991), and b) the presence of seismic anisotropy illustrates that dislocation creep is dominant throughout a significant portion of the mantle (Karato and Wu, 1993). The diffusion creep reference viscosity for T_m is therefore chosen to be 10^{20} Pa s, and for dislocation creep, this reference viscosity is reached for a so-called 'transition strain rate' $\dot{\varepsilon}_{tr}=1.52\times10^{-14}\,s^{-1}$. This strain rate value is slightly lower than the typical plate-driven upper mantle convection strain rate, and will therefore result in dislocation creep as the dominant creep mechanism. Published values for E^* vary significantly between ~240 and ~540 kJ/mol, depending on material, deformation mechanism, and water content (cf., Karato and Wu, 1993), and an average value of $E^*=360$ kJ/mol is used. n is taken from dry

dislocation creep values in (Karato and Wu, 1993). For yielding, a friction coefficient $\mu=0.1$ provides good subduction dynamics in models with a free-slip top boundary condition and freely subducting plates (e.g., Di Giuseppe et al., 2008; Enns et al., 2005), and is in tune with estimates for active faults (Collettini et al., 2009). However, these constraints leave room for some rheological uncertainty. For example, the viscous strength of both diffusion and dislocation creep is affected significantly by the presence of water (e.g., Hirth and Kohlstedt, 2003; Korenaga and Karato, 2008). Therefore, we will investigate the effects of variation of the most dominant rheological model parameters to investigate their effect. Similar to previous work (Andrews and Billen, 2009; Gerya et al., 2004),elastic deformation is not considered, since, at the ambient p–T conditions of slab break-off, any elastic stresses will have relaxed during break-off.

In the models, the same rheology is assumed for mantle and crustal rocks without any internal rheological layering in the lithosphere. However, the viscous strength for crustal material is probably lower than for mantle material (Kohlstedt et al., 1995), and therefore, such simplified lithosphere rheology ignores the potential crust–mantle lithosphere decoupling and delamination processes (e.g., Ranalli et al., 2005) that could promote ongoing subduction of mantle lithosphere. Although possibly important for Himalayas and Alps where long-term continued convergence is observed (Royden, 1993), this is not the focus of this work. To account for the effects of thinned subducted crust, we vary crustal thickness of the subducting continental block.

Subduction is enabled by a narrow static weak zone (~10 km wide with a uniform viscosity of 10^{20} Pa s) to the base of the lithosphere, and a weak mantle wedge underneath (of approximately 100 km deep and 200 km wide, situated above the slab, and also with a uniform viscosity of 10^{20} Pa s), which together decouple the subducting from the overriding plate. Such approach allows for convergent plate decoupling without the complexities of slab dehydration and mantle wedge hydration and weakening, but doesn't affect the slab break-off process. The 3-D models also have weak transform faults at $y=330$ km and $y=2310$ km with the same width and weakness as the subduction fault to decouple the subducting plate from its neighbouring plates in the y-direction. This creates a subducting slab of finite width only between those transform faults, avoids possible interaction of the slab edge with the sides of the computational domain, and allows for possible mantle flow around the slab edges. In this model setup, the position of the overriding plate and weak zones is fixed with respect to the underlying mantle, which implies that slab roll back and trench motion are not occurring. This is likely to affect the shape of the subducting plate, since slab roll back promotes shallow dip angles and prevents turned-over slabs, but no first-order effect on the dynamics of slab break-off is expected.

2.3. Governing equations and computational aspects

The 2-D and 3-D flow calculations are performed with a Cartesian version of the finite element code Citcom (Moresi and Gurnis, 1996; van Hunen et al., 2005; Zhong et al., 2000). The code assumes incompressible flow, and adopts the Boussinesq approximations. The non-dimensional governing equations are described by the following equations for the conservation of mass, momentum, and energy, and composition:

$$\nabla\cdot u = 0 \tag{4}$$

$$-\nabla P + \nabla\cdot\left(\eta\left(\nabla u + \nabla^T \boldsymbol{u}\right)\right) + (RaT + RbC)\boldsymbol{e_z} = 0 \tag{5}$$

$$\frac{\partial T}{\partial t} + \boldsymbol{u}\cdot\nabla T = \nabla^2 T \tag{6}$$

$$\frac{\partial C}{\partial t} + \boldsymbol{u}\cdot\nabla C = 0 \tag{7}$$

with symbols defined in Table 1, the thermal Rayleigh number Ra defined in the usual way for bottom-heated convection:

$$Ra = \frac{\alpha\rho_0 g\Delta T h^3}{\kappa\eta_0}, \tag{8}$$

and the compositional Rayleigh number Rb defined in a similar way:

$$Rb = \frac{\delta\rho_c g h^3}{\kappa\eta_0}, \tag{9}$$

with $\delta\rho_c=600$ kg/m^3 the compositional density difference between mantle material and continental crust. A standard non-dimensionalisation is applied (McKenzie et al., 1974), using $x=x'h$, $t=t'h^2/\kappa$, $\eta=\eta'\eta_0$, and $T=T'\Delta T$. The primes are dropped in the equations above and the remainder of the paper for clarity.

Eqs. (4) to (6) are solved with using a finite element technique (see Moresi and Solomatov, 1995 for more details), and an iterative conjugate gradient solver. Eq. (7) (conservation of composition) is solved using a particle-tracing technique, where a dense set of particles is advected with the flow, and carries the compositional information (Ballmer et al., 2007; Di Giuseppe et al., 2008; van Hunen et al., 2002). The implementation of particle advection and interpolation is benchmarked against van Keken et al. (1997) and in Schmeling et al. (2008). Bilinear interpolation is used to interpolate tracer values to the nodal points of the orthogonal finite element mesh.

The necking process that results in slab break-off involves localized deformation, and it is useful to know how this process is resolved numerically. For all shown calculations, the finite element resolution varies between 3.5 km and 10 km in each direction for all 2-D and 3-D calculations. The highest resolution is applied to the core area where plate decoupling, subduction and slab break-off occur, and the lower resolution is applied outside this area. As a resolution test, the default model (Fig. 2) was repeated with model *hr*, which has twice the resolution in each direction, and resulted in 13% shorter Δt_{br}, the delay time between continental collision and slab break-off, one of the main characteristics in this study (see Figs. 2 and 4 for further details). This difference is primarily caused by the difference in decoupling of the converging plates in the subduction weak zone: a higher resolution results in more plate decoupling, faster convergence, and consequently earlier break-off. How resolution affects the actual necking process (the focus of this study), is indicated by an *hr* model calculation with a similar amount of plate decoupling as the default calculation. In that case, Δt_{br} for the hr model is 4.8% shorter than for the default calculation. A uniform density of randomly distributed particles is chosen high enough to ensure a minimum of 40 particles for even the smallest finite elements.

3. Results

We aim to study the intrinsic differences between 2-D and 3-D slab break-off. To give insight in the general process of slab break-off, and to enable a detailed model parameter study, we will first discuss 2-D calculations. These results can be put in the context of previous work, and will provide a reference for the next section that describes full 3-D models, which enables intrinsically 3-D processes such as lateral slab tear migration.

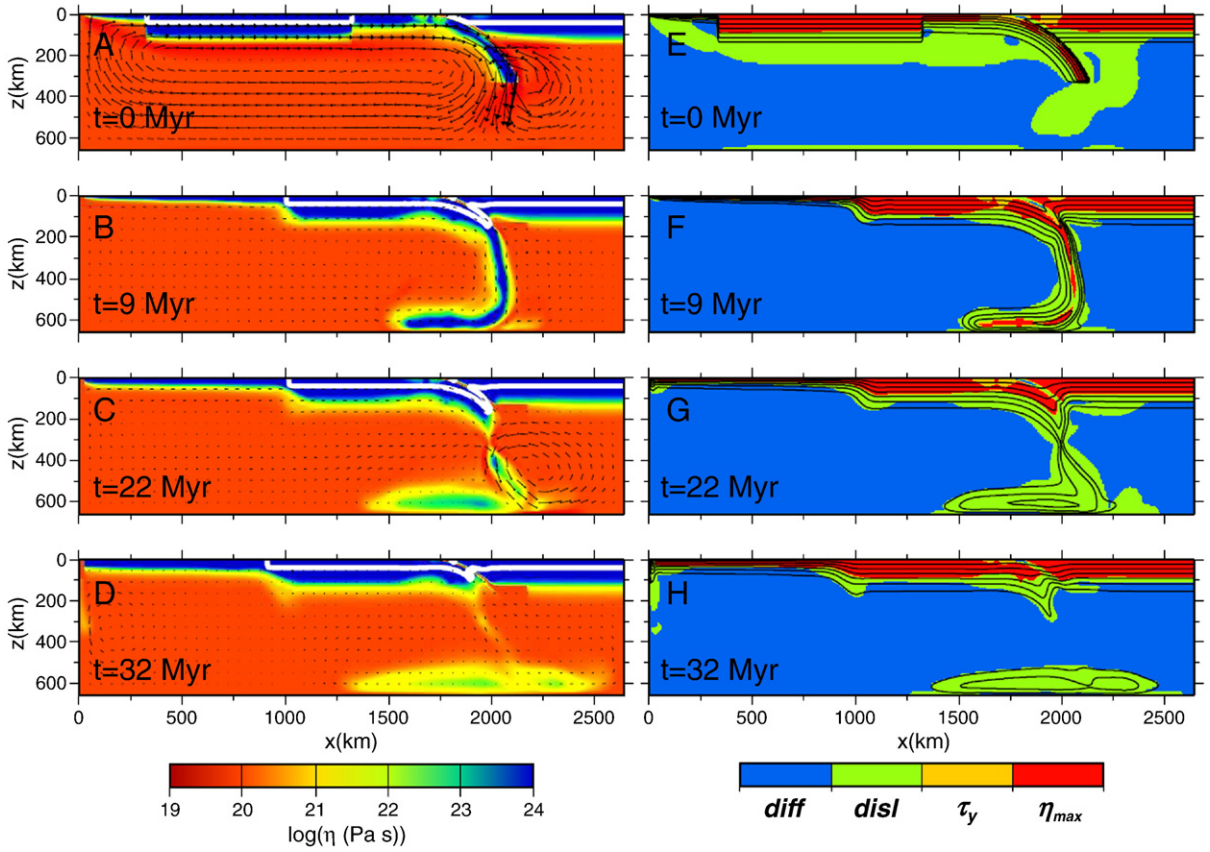

Fig. 2. A–D) Illustration of the process of continental collision and subsequent slab break-off by illustrating (in colour) the effective viscosity, the location of the buoyant continental crust (outlined in white), and plate/mantle motion (arrows). High viscosity marks the lithosphere and slab, whereas the mantle has a low viscosity, especially around and during slab break-off. A) Initial condition at model time $t=0$, where convergence is enabled by a narrow low-viscosity fault zone. B) Subduction significantly slows down and eventually stops when the continental block collides with the subduction zone at model time $t=9$ Myr. C) $t=21$ Myr: the previously subducted slab warms up and eventually breaks and sinks into the mantle. D) $t=32$ Myr: afterwards, the partly subducted continental crust slowly 'exhumes' towards a new equilibrium depth. E–H) Model times correspond to panels A–D, respectively. The distribution of the dominant (i.e. weakest) deformation mechanism (in colour) illustrates that during break-off, most of the mantle is deforming by diffusion creep, but the break-off itself occurs in the dislocation creep regime. Contour lines illustrate the temperature distribution (contours every 200 K).

3.1. 2-D results

The basic continental collision and slab break-off process is illustrated using the default 2-D model: a 60-Myr old oceanic plate contains a 150-km deep continental block with a 40-km thick continental crust with a 600 kg/m^3 lower density than mantle material for the same temperature. Default rheological parameters are described in the previous section and Table 1. Figure 2 shows the evolution of continental collision and slab break-off with a time series of effective viscosity distributions. Initially, a slab is situated halfway into the upper mantle. The continental block is characterized by a relatively thick rheological lithosphere and a buoyant continental crust, and initially is separated from the overriding continent by a 400 km wide oceanic basin. As subduction proceeds, the slab lengthens and slab pull increases, which leads to faster subduction (Fig. 3). When the slab reaches the base of the model at 660 km depth, it becomes supported from below, which results in a drastic drop in subduction velocity. Eventually, the slab will buckle, and will continue its descent until the continental block approaches the subduction zone. Upon entering the subduction zone, the thick, buoyant crust of the continent resists subduction, and the convergence rate drops significantly (Fig. 3), until the continental crust has entered the trench to a maximum depth of 186 km (Fig. 2) at around 12.5 Myr after the initial collision.

Slab break-off occurs in the part of the slab where tensile stresses are the largest. Shallower parts of the slab experience more tensile stress, because the weight of the hanging part of the slab below is larger. But the continental block is thicker and therefore stronger than the oceanic part, and therefore better resists breaking. As a consequence, the slab will break off at the oceanic side of the previous 'passive margin'. Continental subduction instantaneously increases the tensile stress at the transition between the dense oceanic slab and the buoyant continental block, but it takes 16.5 Myrs from the moment of continental collision before the slab breaks off.

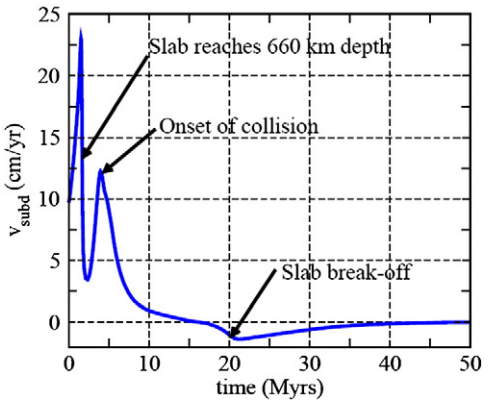

Fig. 3. Subduction velocity evolution for model 1, measured as the horizontal plate motion of the subducting plate just before it enters the trench. Initially high subduction velocities (due to the freely falling short slab) are reduced when the slab reaches the base of the upper mantle. Subduction velocities further decay when the continental block enters the subduction zone, until around 16 Myrs, the slab breaks off, and the continental block experiences a negative 'exhumation' velocity.

So there is a significant time of (about 4 Myr for this default model) between the moment of maximum crustal burial and the time of slab break-off. Apparently the increased tensile stress is in itself not sufficient to immediately break the slab. Instead, slab break-off is a longer-term process in which the slab warms up to about 800 °C (Fig. 2), which reduces the (temperature-dependent) viscosity. During this break-off process, the slab is gradually losing coherence and the shallow, buoyant continental part is beginning to decouple from its deeper counterpart, and is starting its 'exhumation'. Localization of the deformation or 'necking' of the slab takes place: the slab starts to stretch in the part which is weakest, or which experiences the largest vertical tensile stress; this stretching makes the slab locally shorter in horizontal direction, and makes this part of the slab weaker than the rest, and more vulnerable to further stretching, and so on. This eventually leads to a localized detachment of the slab from the overlying continental block. The slab then sinks down into the mantle at several cm/yr, while the continental block experiences a small 'exhumation' event, illustrated by the negative subduction velocity (Fig. 3). The first break-off occurs at a depth of ~300 km, but subsequent exhumation of the continental block and sinking of the detached slab leads to a slab window that extends from ~200 km to the transition zone.

Figure 2E–H illustrates that the dominant deformation mechanism at and around the location of break-off is dislocation creep. This is because the ambient stress and strain rates are relatively large in this area, which lowers the dislocation creep strength to values below the 'background' diffusion creep strength. The dislocation creep regime is modestly strain-localizing (e.g., Bercovici, 2003), and leads to necking and localized break-off. Especially in the immediate vicinity of the break-off location, strain rates are high, which leads to effective viscosities locally as low as 2×10^{19} Pa s, a factor of 5 lower than the ambient mantle away from the subduction zone. A stress limiting rheology applies to this model, with a yield stress of 400 MPa. Yielding plays a role in the deformation of the plate and slab during 'normal' subduction, but this deformation mechanism is not dominant at and around the location and time of break-off (Fig. 2G). Instead, dislocation creep dominates the deformation near slab break-off. This was observed not only in the default model, but in all the model calculations. Apparently, tensile stresses in the subducted slab after collision are not large enough to reach the yield strength.

3.2. 2-D model parameter sensitivity

This section aims to provide insight in the robustness of the collision–break-off process and the sensitivity of various model parameters. We first vary parameters that define the subducting plate, and then examine the influence of rheological settings.

The age of the oceanic part of the subducting plate at the subduction zone (age_{plate}) has been varied between ~35 Myr and ~90 Myr (default is 60 Myr) at the start of the model calculation, which results in an oceanic plate cooling halfspace thickness (Turcotte and Schubert, 2002) at the trench of ~60 and ~100 km, respectively (Fig. 4). Plate age affects both the available amount of slab pull of the system, and the strength of the subducting plate. An older oceanic plate is able to drag down its trailing continental block with buoyant continental crust for longer (Fig. 4A, black curve), and to larger depth (Fig. 4D). After plate convergence has ceased, the strength of the slab delays the eventual break-off by several Myrs (Fig. 4A, red curve). This delay is larger for older slabs (as shown by the longer time span between the moment of maximum crustal burial to the break-off event), because the older slab is thicker and stronger and needs more heating time to become weak enough to break. Despite the differences in model setup, these results qualitatively correspond with those by Gerya et al. (2004). The somewhat anomalous points in Figure 4A,D for a 45 Myr-old plate mark a change towards a slab folding onto itself (as shown in Fig. 2B, see also Di Giuseppe et al., 2008), which is promoted by the static trench location in our model setup.

The thermal thickness of the continental block (d_{cont}) (defined as the depth where the continental geotherm reaches the mantle temperature) is varied between 100 and 200 km (default is 150 km) (Fig. 4B,E). The effect of this variation shows several similarities with oceanic plate age variation. A thicker continental block partly compensates the crustal buoyancy with its additional thermal weight, and is therefore able to subduct deeper (Fig. 4E), and for a longer time (Fig. 4B, black curve). Consequently, slab break-off also occurs deeper. But unlike the oceanic plate age variation in Figure 4A, the break-off

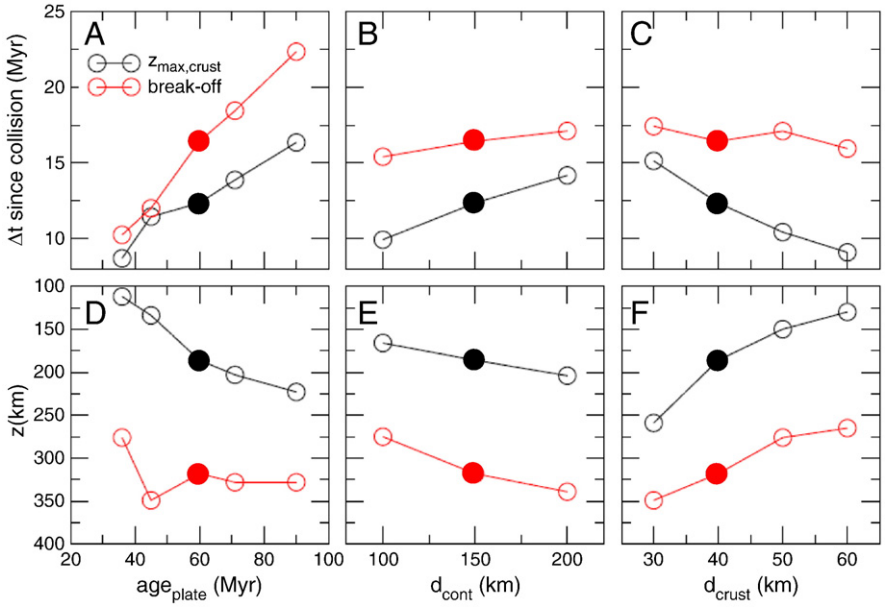

Fig. 4. Delay time since collision (A–C) and depth (D–F) of maximum crustal burial (black) and break-off (red) reached during each model calculation for varying model parameters. Collision timing is defined as the moment when leading edge of the continental block reaches the trench at $x=1782$ km. Depth and timing of break-off is defined by the location and moment of the maximum vertical stretching $\frac{dv_z}{dz}\big|_{max}$. The model parameters shown here are the lithospheric age at subduction (A,D), the thickness of the continental block (B,E), and thickness of the crust in the continental block (C,F). Solid symbols refer to the default calculation from Figures 2 and 3.

time is much less affected by continental thickness variation. This reflects the fact that slab break-off occurs within the oceanic part of the slab, and not within the continental block, and the timing of break-off is mostly determined by the heat-up time of the oceanic plate.

Figure 4C,F illustrate the effect of changing crustal thickness d_{crust} within the buoyant continental block, varying d_{crust} between 20 and 60 km (default is 40 km). A thin crust is less buoyant than a thick one, so that an oceanic slab can drag down the continental block with thin crust deeper until neutral buoyancy will stop further convergence. This also leads to deeper slab break-off, and since it takes longer to drag the continent deeper, the moment of maximum crustal burial is also later in this case. For calculations with $d_{crust}=20$ km, the continental block subducted completely without collision or slab break-off. As for the case of continental thermal lithospheric thickness variation, the timing of break-off is little affected by the thickness of the crust in the continental block.

Variation of rheological parameters gives insight in the role of plate and mantle strength in the process of slab break-off. To this end, we varied the maximum yield strength, the rheological prefactors A (see Eq. (1)) for both diffusion and dislocation creep, and the strength of the subduction weak zone (Fig. 5).

Maximum yield strength τ_{max} is varied between 200 and 1000 MPa (default is 400 MPa) (Fig. 5A,D). Increasing τ_{max} to values above the default 400 MPa has little effect on the maximum crustal burial, and the depth of break-off. This further confirms that around the area of slab break-off, the dominant deformation mechanism is not yielding, but dislocation creep. For lower yield strength, however, the influence of yielding becomes larger. This manifests itself in shallower crustal burial (the slab is too weak to drag down the trailing buoyant continental block). The variation in timing of the deepest crustal burial for the cases with $\tau_{max}>200$ MPa relates to the shape of the slab in the upper mantle, and how it folds onto itself, which influences the subduction velocity and the slowdown after collision. So yield strength influences the slab dynamics, and therefore indirectly the timing break-off. But, as shown in Figure 2G, yielding does not occur at the time and location of slab break-off. This result differs from those in Andrews and Billen (2009), probably mostly because of the reduced tensile stress in the slabs in this study, which are fully supported at the base of the transition zone.

Changing the material strength in the dislocation creep regime A'_{disl} (Fig. 5B,E) around its unity default value has a significant effect on the timing of break-off. This is expected as the dominant deformation regime around break-off is dislocation creep. A change from −50% to +50% in the prefactor A (Eq. (1)) can result in a break-off delay after collision ranging from 10 to 20 Myr, comparable to the effect of changing the slab age by ±30 Myr. Changing the dislocation creep strength has little effect on the depth of maximum crustal burial or slab break-off.

The effects of changing the diffusion creep strength A'_{pref} around its default value of unity are minimal (Fig. 5C,F). This reflects the fact that neither deformation in the general subduction dynamics (mostly plate bending and unbending) nor the break-off process is dominated by diffusion creep deformation.

Finally, changing the strength of the viscosity weak zone η'_{wz} around its default value of one has no significant influence on the maximum crustal burial or depth of break-off, but has a significant influence on the timing on these events. The moment of maximum crustal burial is accelerated by the faster convergence for the weaker subduction zone. After this maximum burial, break-off is enhanced by 'exhumation' while continental block decouples from the subducted slab. This exhumation is faster for the weaker subduction zone. This illustrates that the coupling between subducting and overriding plates is an important parameter in the process of slab break-off.

These 2-D parameter sensitivity studies illustrate two important general results. First, the dynamics of the transition from subduction to collision plays an important role in the slab break-off process, because it is responsible for the tensile stress variations in the slab. Second, it shows that plate strength is important for the delay time between continental collision and slab break-off. This is mainly for two reasons: a) the strength of the slab determines how long it needs to warm up before it is weak enough to break, and b) the plate strength influences the 'collision speed', i.e. the average convergence rate of the two plates after collision has started, which in, in turn, influences how long after initial collision the subduction process has completely stopped.

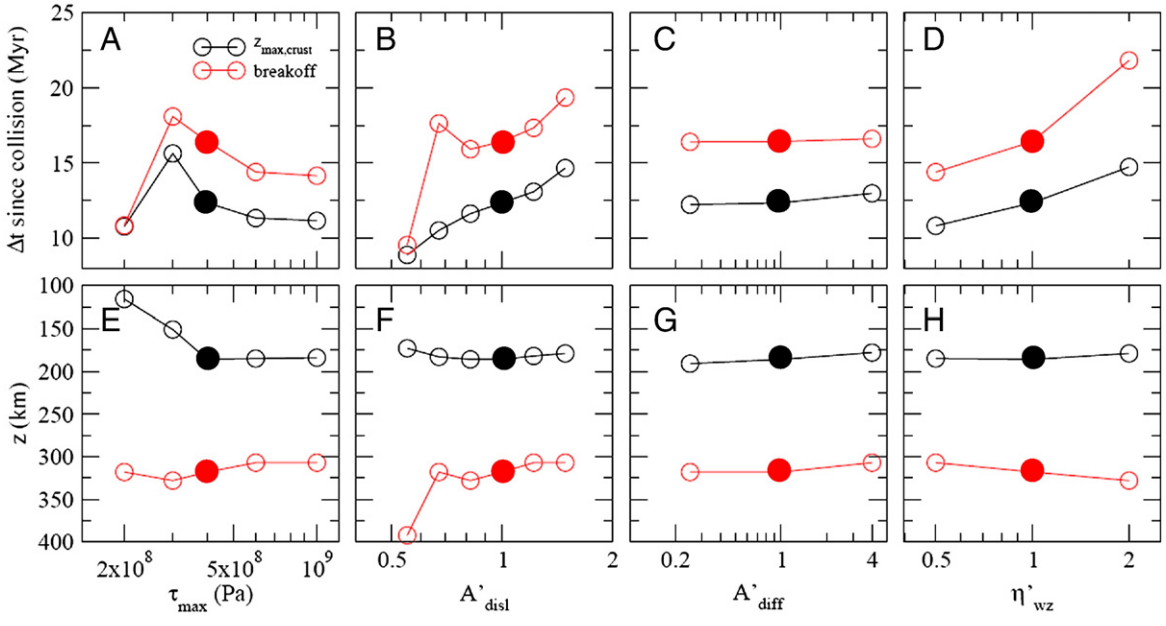

Fig. 5. As Figure 4, but for variation of rheological parameters. The model parameters shown here are the maximum yield strength τ_{max} (A,E), dislocation creep strength relative to the default model A'_{disl} (B,F), the diffusion creep strength relative to the default model A'_{diff} (C,G), and the subduction weak zone viscosity relative to the default model η'_{wz} (D,H). Solid symbols refer to the default calculation from Figures 2 and 3.

Many additional parameters could play a role in the break-off dynamics, both physical parameters (such as more complex mineralogy) and model parameters (such as the applied initial and boundary conditions), although these are not likely to have larger influence than the ones investigated here. Overall uncertainty estimates are difficult to make for the results presented in this section, but the presence of such uncertainties should be kept in mind when model results are compared to observations.

3.3. 3-D collision, slab break-off, slab windows, and tear migration

Next, continental collision in a 3-D setting is elaborated and discussed. We start with a model, in which the subducting plate is limited in width (i.e. in *y*-direction, which is the direction perpendicular to the previously discussed 2-D models), but no other variation in *y*-direction is imposed. A continental block covers the subducting plate over its full *y*-range. Figure 6 illustrates this scenario during the break-off of the slab after collision of the continental block.

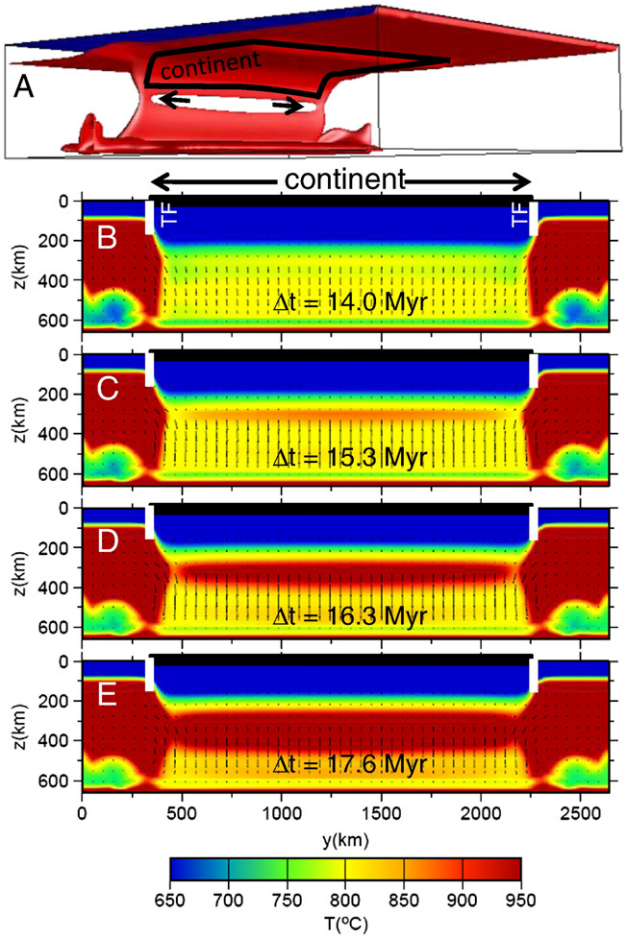

Fig. 6. A) 3-D illustration of the subducting slab after collision during the slab break-off process, with the 945 °C-isotherm in red, and the surface in blue. The slab starts breaking in the middle, and a 'tear' is propagating towards the edges of the slab. The position of the continent is outlined in black. B–E) Illustration of 3-D slab break-off in a trench-parallel view through the slab. Colours indicate the presence of slab material at any *x*-coordinate by plotting the lowest temperature over a range of *x*-coordinates that span the *x*-location of the slab. So any dark-red colour in the plots indicates that no temperatures lower than 950 °C are present at this (*y*,*z*)-coordinate. The location of the continent and transform fault (TF) is schematically illustrated with the black and white bars, respectively. This model has a continent entering the subduction zone along the entire trench between the transform faults. Elapsed time Δt since onset of collision: B) 14.0, C) 15.3, D) 16.3, and E) 17.6 Myrs. As discussed in the text, slab break-off first occurs at the slab interior as a slab window and slightly later at the slab edges.

Slab break-off in this model starts in the middle of the slab as a slab window, and then propagates outwards towards the edges of the slab. Given that collision occurs simultaneously along the full length of the slab, it may seem surprising at first that break-off doesn't occur simultaneously as well. The reason for that is that necking in 3-D differs from necking in 2-D. To conserve mass in 2-D necking, the vertical stretching of the slab approximately equals the amount of horizontal shortening. In 3-D, vertical stretching is accommodated by shortening in two horizontal directions, and therefore horizontal shortening in each of those horizontal directions is only approximately half that of the 2-D scenario. So necking is slower at the edges, and therefore localizes towards the slab interior. In the middle of the 3-D slab (i.e. away from one of its edges in *y*-direction), there is very little model variation in the *y*-direction, and the slab roughly behaves as in the 2-D models: vertical stretching is accommodated by shortening in *x*-direction. But at each end of the slab, vertical stretching is accommodated by shortening in *x*-direction and *y*-direction. This can be seen in Figure 6B–E from the slab shortening in *y*-direction at the depth of break-off, and from the clockwise (anticlockwise) velocity arrows at the left (right) edge of the slab.

Figure 6 furthermore illustrates the time evolution of this 3-D slab break-off scenario. The timespan between initial rupture and completion of the break-off process is on the order of 1.5 Myr, which illustrates that the approximate delay time of break-off at slab edges compared to slab interiors is only very small, and perhaps insignificant in comparison to the total duration of the collision-to-break-off process. Furthermore, it is not useful to translate these delay times in a tear propagation rate, since this delay time is almost independent of the width of the slab: a twice as wide slab would show necking in its entire interior almost simultaneously, and only the edges would take longer to break off. More importantly, this scenario illustrates that slab break-off doesn't necessarily need to initiate at a slab edge.

Although a 3-D model without lateral variation in the slab is insightful, a more common scenario is that only part of the subduction zone is choked by continental collision, while adjacent to that oceanic subduction continues. In Figure 7, results are shown for a model, in which 2/3 of the subducting plate has a continental block embedded, while the remaining 1/3 has no continental block, and is purely oceanic. Upon collision, this asymmetry leads to resistance against subduction at the side of the continental block, while on the other side oceanic subduction continues. This leads to a slight rotation of subducting plate (counter-clockwise in plan view) and to a larger vertical tensile stress on the 'continental' edge of the slab. Therefore, the slab first breaks on that side, although the effect of 3-D necking is still visible (Fig. 7C). This first break-off occurs around 16.5 Myrs (i.e. at the delay time after collision similar to the default 2-D case, and the 'symmetric' 3-D case), and the break-off below the continental block is complete by ~20 Myrs, i.e. ~3.5 Myrs later. Over this time, the tear propagates over 1000–1200 km, which suggests an average tear propagation rate of about 300 mm/yr.

To investigate the sensitivity of the tear propagation rate to variations in model parameters, the most influencing plate and rheological parameters in the previously discussed 2D models were varied in a series of 3D model calculations as well. Results are shown in Figure 8. As for the 2-D models, the age of the subducting plate plays an important role in the resulting tear propagation rate, and the 30-cm/yr rate as observed in the default asymmetric 3-D model (Fig. 8) varies from 125 mm/yr (90 Myr slab) to 800 mm/yr (35 Myr-old slab). The reason for this variation is the same as for the delay between collision and break-off: older slabs are stronger, and therefore more difficult to break, which results in a slower tear propagation. Varying the dislocation creep strength by ~50% results in a change in tear propagation rate up of about 100 mm/yr, or approximately 30%. This illustrates that the applied rheology is not unimportant for the expected tear propagation rate, but that the oceanic slab age at the time of subduction is probably the more important parameter.

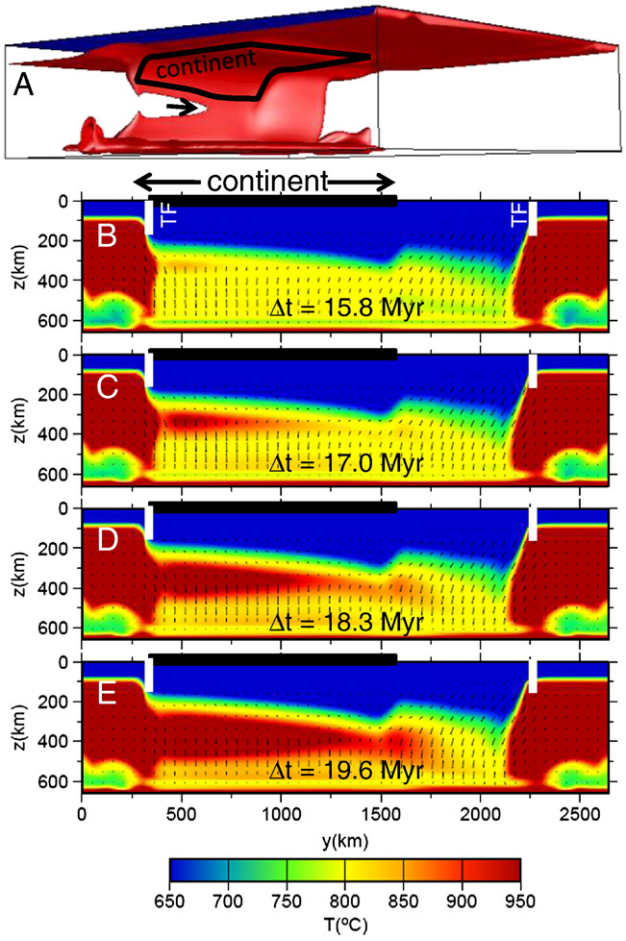

Fig. 7. As Figure 6, but for a model, in which only part of the slab has a continental block. A) Slab break-off starts near the continental edge of the slab and propagates towards the opposite edge. B–E) Illustration of 3-D slab break-off in a trench-parallel view through the slab for different times Δt since collision: B) $\Delta t = 15.8$ Myr, C) $\Delta t = 17.0$ Myr, D) $\Delta t = 18.3$ Myr, E) $\Delta t = 19.6$ Myr. The slab starts breaking near its left edge, and a tear propagates towards the other end of the continental block with an average velocity of 300 mm/yr.

4. Discussion

4.1. Slab tear propagation rates

Using a fully dynamic 3-D numerical model of subduction–continental collision, we are able, to our knowledge for the first time, to quantify the process of 3-D lateral slab break-off. When asymmetry is introduced, by using a continental block of limited trench-parallel extent, the slab break-off propagates laterally with velocities between

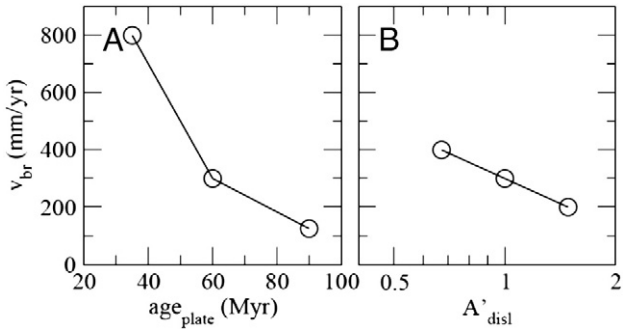

Fig. 8. Slab break-off tear propagation speed plotted against A) subducting plate age and B) relative dislocation creep strength.

100 mm/yr (old, strong slabs) and 800 mm/yr (young, or weak slabs). This falls within the wide range of previous estimates of 20–940 mm/yr from theoretical calculations based on 3-D stress models (Yoshioka and Wortel, 1995) and depocentre migration in the Carpathians of 70–450 mm/yr (Meulenkamp et al., 1996). Our results further illustrate that even in the case of simultaneous collision along the whole trench, slab break-off shows lateral migration, where the slab starts breaking in the middle and a tear propagates outwards. This illustrates that slab break-off doesn't necessarily start at the edge of a slab, and that break-off preferably commences at a slab interior because thermal necking of the slab is slower at the slab edge. The large variation in both our and published propagation rates is partly reflected by the difficulty to define this tear propagation. Since slab break-off at any point in the slab is not instantaneous, but typically evolves on a Myr timescale, and tear propagation is rapid and sweeps over the width of the continent in just a few Myrs, defining tear propagation rates is difficult, and recognizing its observables perhaps even more so.

4.2. Application to the Arabia–Eurasia collision zone

The presented results can be used to put novel constraints on the evolution of the Arabia–Eurasia collision, which followed northwards subduction of the Neo-Tethyan Ocean under the southern margin of Eurasia.

Seismic tomography has revealed the presence of velocity anomalies in the mantle under southwest Asia (Bijwaard et al., 1998; Hafkenscheid et al., 2006), interpreted as primarily caused by temperature variations. The variation is consistent with the presence of a detached slab of Neo-Tethyan oceanic lithosphere beneath the collision zone. Other parameters related to this slab are not well known, including the time of break-off, the rate of lateral migration (if any) and the rate of descent in to the mantle. Geological parameters are known with varying degrees of certainty. There is general agreement that the opening of the Neo-Tethys began in the Late Permian (e.g., Sengör et al., 1988) which means that the crust entering the subduction zone just before continental collision was ~200 Myr old. This is true regardless of the exact age of initial collision, which is debated. Common estimates are Late Eocene (~35 Ma; Allen and Armstrong, 2008) and Early Miocene (Okay et al., 2010), although these are within a spectrum ranging from the Late Cretaceous/Paleocene (70–60 Ma, e.g., Mazhari et al., 2009) to the mid Miocene (~12 Ma, Guest et al., 2006). A possible compromise is initial collision at ~35 Ma, given the structural, magmatic and stratigraphic changes at that time documented in Allen and Armstrong (2008), followed by an intensification at ~20 Ma (Ballato et al., in press).

Post-collision surges in magmatism and/or surface uplift have been used to infer the presence and time of slab break-off, but again there is no clear consensus. Different authors suggest a different timing of break-off: Middle Eocene, around 40 Ma (Ghasemi and Talbot, 2006), Late Eocene/Early Oligocene, 35–33 Ma, (Dargahi et al., 2010), Mid Miocene (~11 Ma, (Keskin, 2003), and Late Miocene, ~10–5 Ma (Omrani et al., 2008). However, the Middle Eocene magmatic flare-up is likely to relate to back-arc extension in SW Eurasia (Vincent et al., 2005) and so is pre-collisional. There has been an increase in magmatism in the last few million years, with new centres established across eastern Turkey and Iran (Boccaletti et al., 1976; Keskin et al., 1998; Kheirkhah et al., 2009; Shabanian et al., 2009; Walker et al., 2009).

Our model predicts slab break-off as long as 25 Myr after initial continental collision, given the likely 200 Myr age of the slab. This fits a scenario with initial continental collision at ~35 Ma and a slab break-off at 10 Ma, promoting the young and active magmatism across the collision zone.

Hafkenscheid et al. (2006) presented a preferred model of initial break-off at ~30 Ma, based on the prediction that slab-breakoff occurred 10 Myr after initial collision (following the model results of van de Zedde and Wortel, 2001), and the assumption that collision

itself took place at 40 Ma (Dercourt et al., 1993). This Oligocene age was a time of little magmatism across the collision zone, making it unlikely, unless slab break-off occurred with no contribution to melting.

4.3. Break-off depth, STEP faults and slab roll-back

In our numerical models, slab heating and resulting weakening is an important process towards slab break-off. Such heating is more efficient at depth where the slab is fully submerged in the hot mantle than close to the surface, where the slab still lies adjacent to the cold overriding lithosphere. Furthermore the viscous weak zone between the subducting and overriding plate relaxes the tensile stresses in the slab. For these reasons, all slab break-off in this study occurs deeper than ~200 km. This is in contrast to previous studies that discuss shallow slab break-off (as shallow as 30 km) as a mechanism for break-off related magmatism, where a shallow break-off would result in a shallow slab window and subsequent sudden heating and partial melting of the cold overriding lithosphere (Davies and von Blanckenburg, 1995; van de Zedde and Wortel, 2001). Very young subducting slabs and the subduction of mid-ocean ridges might break off shallower (Burkett and Billen, 2009).

Govers and Wortel (2005) and Wortel et al. (2009) discuss the presence of STEP (Subduction-Transform-Edge-Propagator) faults when subduction of oceanic lithosphere rolls back along the margin of a continental block, such as proposed for the Southern Apennines (Faccenna et al., 2009; Wortel and Spakman, 2000). In such geometry, the tearing between the subducting oceanic part of the plate and the non-subducting continental part would decouple those parts, and allow continued subduction and roll-back of the oceanic part of the subducting plate, thereby potentially reducing the stress in the continental block and delaying break-off. Such tear would necessarily extend throughout the whole subducting plate all the way to the surface. The effects of STEP faults or slab roll-back on the tear migration rates are not included in this study, and remain to be investigated.

4.4. Secular evolution of continental collision since the Archaean

Finally, we briefly discuss possible implications for the occurrence and style of subduction and subsequent continental collision in the early Earth. Ultra-high pressure metamorphism (UHPM) and blueschists are a result of subduction of continental crust to large (>100 km (e.g., Maruyama and Liou, 1998) depth, and subsequent exhumation of this crust back to the surface. UHPM and blueschists are common in Phanerozoic subduction settings, but appear to absent in Proterozoic and Archean geological records (Brown, 2008; Maruyama and Liou, 1998). This has been attributed to a change in the style of subduction (Brown, 2008), or even absence of plate tectonics (Stern, 2005). We hypothesize that this evolution is due to secular changes in plate strength. Our results illustrate that the timing and depth of maximum burial of continental crust and slab break-off varies significantly with the age of the subducting plate, the material yield strength and the dislocation creep strength. In general, this shows that a weaker oceanic plate cannot drag down a buoyant continent as much as a strong plate. In the Early Earth, when the mantle was 100–300 K warmer, when oceanic crust was thicker, and subduction perhaps faster (Faccenna et al., 2009; Herzberg et al., 2010; van Hunen et al., 2008), oceanic plates might, on average, have been significantly weaker (e.g., van Hunen and van den Berg, 2008). The results presented here show that in this case, the weak slabs in a continental collision setting would have led to earlier and shallower break-off than collision would today, when slabs are stronger. So continental crust would not reach the depth required to form blueschists and UHPM, and would therefore be absent in the Precambrian geological record.

5. Conclusions

We used novel 2-D and 3-D fully dynamical models to investigate the self-consistent dynamics of slab break-off after continental collision. Our results indicate that:

1. Slab break-off is viable, even when slabs are supported from below by the spinel-to-perovskite phase transition and a strong lower mantle;
2. Delay time between the first continental collision and the occurrence of slab break-off depends mostly on the strength of the previously subducted oceanic plate, and ranges from 10 Myr (for young, weak slabs) to >20 Myr (for old, strong slabs);
3. Slab break-off has a weak preference to start in the slab interior, and not on the slab edge, due to the nature of slab necking. But any asymmetry in the collision process will override this, and will lead to a tear propagating from one edge of the slab to the other;
4. Slab tear propagation rates range from <150 mm/yr for old, strong oceanic slabs to ~800 mm/yr for a 35-Myr oceanic slab.

These results are used to constrain the timing of the Arabia–Eurasia collision, and proposed subsequent slab break-off. Given the previous subduction of the old Neo-Tethyan slab, a large delay time between collision and break-off is expected, which argues for relatively recent (~10 Ma) slab break-off.

Finally, the relatively rapid break-off for young, weak slabs has implications for the collision-related ultra-high pressure metamorphism. Early break-off limits the depth extent of burial of continental crust, which provides an explanation for the absence of this metamorphism in the Proterozoic and Archaean, when the mantle was hotter and slabs weaker.

Acknowledgments

The authors would like to thank Susanne Buiter and an anonymous reviewer for their detailed and constructive reviews that significantly improved the manuscript. JvH would like to thank Claudio Faccenna, Rob Govers, Wim Spakman, Jack Barnard, Valentina Magni, and Rinus Wortel for inspiring discussions.

References

Allen, M.B., Armstrong, H.A., 2008. Arabia–Eurasia collision and the forcing of mid Cenozoic global cooling. Palaeogeogr. Palaeoclimatol. Palaeoecol. 265, 52–58.
Andrews, E.R., Billen, M.I., 2009. Rheologic controls on the dynamics of slab detachment. Tectonophysics 464 (1–4), 60–69.
Ballato, P., Uba, C.E., Landgraf, A., Strecker, M.R., Masafumi, S., Stockli, D.F., Friedrich, A., and Tabatabaei, S.H., in press. Arabia–Eurasia continental collision: insights from late Tertiary foreland-basin evolution in the Alborz mountains, northern Iran. Bulletin of the Geological Society of America. doi:10.1130/B30091.1.
Ballmer, M.D., van Hunen, J., Ito, G., Tackley, P.J., Bianco, T.A., 2007. Non-hotspot volcano chains originating from small-scale sublithospheric convection. Geophys. Res. Lett. 34 (23).
Bercovici, D., 2003. The generation of plate tectonics from mantle convection. Earth Planet. Sci. Lett. 205, 107–121.
Bijwaard, H., Spakman, W., Engdahl, E.R., 1998. Closing the gap between regional and global travel time tomography. J. Geophys. Res. 103, 30055–30078.
Boccaletti, M., Innocenti, F., Manetti, P., Mazzuoli, R., Motamed, A., Pasquare, G., Radicati di Brozolo, F., Amin Sobhani, E., 1976. Neogene and quaternary volcanism of the Bijar Area (Western Iran). Bull. Volcanol. 40, 122–132.
Brown, M., 2008. Characteristic thermal regimes of plate tectonics and their metamorphic imprint throughout Earth history: when did Earth first adopt a plate tectonics mode of behavior? When Did Plate Tectonics Begin on Planet Earth, 440, pp. 97–128.
Buiter, S.J.H., Govers, R., Wortel, M.J.R., 2002. Two-dimensional simulations of surface deformation caused by slab detachment. Tectonophysics 354 (3–4), 195–210.
Burkett, E.R., Billen, M.I., 2009. Dynamics and implications of slab detachment due to ridge-trench collision. J. Geophys. Res. Solid Earth 114, B12402.
Byerlee, J.D., 1978. Friction of rocks. Pure Appl. Geophys. 116, 615–626.
Carminati, E., Wortel, M.J.R., Spakman, W., Sabadini, R., 1998. The role of slab detachment processes in the opening of the western-central Mediterranean basins: some geological and geophysical evidence. Earth Planet. Sci. Lett. 160, 651–655.
Cloos, M., 1993. Lithospheric buoyancy and collisional orogenesis: subduction of oceanic plateaus, continental margins, island arcs, spreading ridges, and seamounts. Geol. Soc. Am. Bull. 105, 715–737.

Collettini, C., Niemeijer, A., Viti, C., Marone, C., 2009. Fault zone fabric and fault weakness. Nature 462 (7275), U907–U998.
Dargahi, S., Arvin, M., Pan, Y.M., Babaei, A., 2010. Petrogenesis of post-collisional A-type granitoids from the Urumieh–Dokhtar magmatic assemblage, Southwestern Kerman, Iran: constraints on the Arabian–Eurasian continental collision. Lithos 115 (1–4), 190–204.
Davies, J.H., von Blanckenburg, F., 1995. Slab breakoff: a model of lithospheric detachment and its test in the magmatism and deformation of collisional orogens. Earth Planet. Sci. Lett. 129, 85–102.
Dercourt, J., Ricou, L.E., Vrielynk, B., 1993. Altas Tethys, Palaeoenvironmental Maps. Elsevier, New York.
Di Giuseppe, E., van Hunen, J., Funiciello, F., Faccenna, C., Giardini, D., 2008. Slab stiffness control of trench motion: insights from numerical models. Geochem. Geophys. Geosyst. 9, Q02014.
Enns, A., Becker, T.W., Schmeling, H., 2005. The dynamics of subduction and trench migration for viscosity stratification. Geophys. J. Int. 160 (2), 761–775.
Faccenna, C., Di Giuseppe, E., Funiciello, F., Lallemand, S., van Hunen, J., 2009. Control of seafloor aging on the migration of the Izu–Bonin–Mariana trench. Earth Planet. Sci. Lett. 288 (3–4), 386–398.
Ferrari, L., 2004. Slab detachment control on mafic volcanic pulse and mantle heterogeneity in central Mexico. Geology 32 (1), 77–80.
Gerya, T.V., Yuen, D.A., Maresch, W.V., 2004. Thermomechanical modelling of slab detachment. Earth Planet. Sci. Lett. 226, 101–116.
Ghasemi, A., Talbot, C.J., 2006. A new tectonic scenario for the Sanandaj–Sirjan Zone (Iran). J. Asian Earth Sci. 26 (6), 683–693.
Gogus, O.H., Pysklywec, R.N., 2008. Mantle lithosphere delamination driving plateau uplift and synconvergent extension in eastern Anatolia. Geology 36 (9), 723–726.
Govers, R., Wortel, M.J.R., 2005. Lithosphere tearing at STEP faults: response to edges of subduction zones. Earth Planet. Sci. Lett. 236 (1–2), 505–523.
Guest, B., Stockli, D.F., Grove, M., Axen, G.J., Lam, P.S., Hassanzadeh, J., 2006. Thermal histories from the central Alborz Mountains, northern Iran: implications for the spatial and temporal distribution of deformation in northern Iran. Geol. Soc. Am. Bull. 118 (11–12), 1507–1521.
Gurnis, M., Hager, B.H., 1988. Controls of the structure of subducted slabs. Nature 335, 317–321.
Hafkenscheid, E., Wortel, M.J.R., Spakman, W., 2006. Subduction history of the Tethyan region derived from seismic tomography and tectonic reconstructions. J. Geophys. Res. Solid Earth 111 (B8).
Hager, B.H., 1991. Mantle viscosity: a comparison of models from postglacial rebound and from the geoid, plate driving forces, and advected heat flux. Glacial Isostasy, Sea-level and Mantle Rheology, pp. 493–513.
Herzberg, C., Condie, K., Korenaga, J., 2010. Thermal history of the Earth and its petrological expression. Earth Planet. Sci. Lett. 292, 79–88.
Hirth, G., Kohlstedt, D.L., 2003. The rheology of the upper mantle wedge: a view from experimentalists. The Subduction Factory. American Geophysical Union, Washington D. C, pp. 83–105.
Isacks, B., Molnar, P., 1969. Mantle earthquake mechanisms and sinking of lithosphere. Nature 223 (5211), 1121.
Kameyama, M., Yuen, D.A., Karato, S.I., 1999. Thermal–mechanical effects of low-temperature plasticity (the Peierls mechanism) on the deformation of a viscoelastic shear zone. Earth Planet. Sci. Lett. 168 (1–2), 159–172.
Karato, S., Wu, P., 1993. Rheology of the upper mantle: a synthesis. Science 260, 771–778.
Keskin, M., 2003. Magma generation by slab steepening and breakoff beneath a subduction–accretion complex: an alternative model for collision-related volcanism in Eastern Anatolia, Turkey. Geophys. Res. Lett. 30 (24), 1–4.
Keskin, M., Pearce, J.A., Mitchell, J.G., 1998. Volcano-stratigraphy and geochemistry of collision-related volcanism on the Erzurum–Kars Plateau, northeastern Turkey. J. Volcanol. Geoth. Res. 85, 355–404.
Kheirkhah, M., Allen, M.B., Emami, M., 2009. Quaternary syn-collision magmatism from the Iran/Turkey borderlands. J. Volcanol. Geoth. Res. 182, 1–12.
Kohlstedt, D.L., Evans, B., Mackwell, S.J., 1995. Strength of the lithosphere: constraints imposed by laboratory experiments. J. Geophys. Res. 100 (B9), 17587–17602.
Korenaga, J., 2006. Archean geodynamics and the thermal evolution of earth. In: Benn, K., et al. (Ed.), Archean Geodynamics and Environments. AGU, pp. 7–32.
Korenaga, J., Karato, S.I., 2008. A new analysis of experimental data on olivine rheology. J. Geophys. Res. Solid Earth 113 (B2), B02403.
Levin, V., Shapiro, N., Park, J., Ritzwoller, M., 2002. Seismic evidence for catastrophic slab loss beneath Kamchatka. Nature 418 (6899), 763–767.
Lorinczi, P., Houseman, G.A., 2009. Lithospheric gravitational instability beneath the Southeast Carpathians. Tectonophysics 474 (1–2), 322–336.
Maruyama, S., Liou, J.G., 1998. Initiation of ultrahigh-pressure metamorphism and its significance on the Proterozoic–Phanerozoic boundary. Isl. Arc 7, 6–35.
Mazhari, S.A., Bea, F., Amini, S., Ghalamghash, J., Molina, J.F., Montero, P., Scarrow, J.H., Williams, I.S., 2009. The Eocene bimodal Piranshahr massif of the Sanandaj–Sirjan Zone, NW Iran: a marker of the end of the collision in the Zagros orogen. J. Geol. Soc. 166, 53–69.
McKenzie, D.P., Roberts, J.M., Weiss, N.O., 1974. Convection in the mantle: towards a numerical simulation. J. Fluid Mech. 62, 465–538.
Meulenkamp, J.E., Kovac, M., Cicha, I., 1996. On Late Oligocene to Pliocene depocentre migrations and the evolution of the Carpathian–Pannonian system. Tectonophysics 266 (1–4), 301–317.
Moresi, L.N., Gurnis, M., 1996. Constraints on the lateral strength of slabs from three dimensional dynamic flow models. Earth Planet. Sci. Lett. 138, 15–28.
Moresi, L., Solomatov, V.S., 1995. Numerical investigation of 2D convection with extremely large viscosity variations. Phys. Fluids 7 (9), 2154–2162.
Okay, A.I., Zattin, M., Cavazza, W., 2010. Apatite fission-track data for the Miocene Arabia–Eurasia collision. Geology 38 (1), 35–38.
Omrani, J., Agard, P., Whitechurch, H., Benoit, M., Prouteau, G., Jolivet, L., 2008. Arc-magmatism and subduction history beneath the Zagros Mountains, Iran: a new report of adakites and geodynamic consequences. Lithos 106 (3–4), 380–398.
Parsons, B., McKenzie, D., 1978. Mantle convection and thermal structure of the plates. J. Geophys. Res. 83, 4485–4496.
Parsons, B., Sclater, J.G., 1977. An analysis of the variation of ocean floor bathymetry and heat flow with age. J. Geophys. Res. 82, 803–827.
Ranalli, G., Martin, S., Mahatsente, R., 2005. Continental subduction and exhumation: an example from the Ulten Unit, Tonale Nappe, Eastern Austroalpine. In: Gapais, D., et al. (Ed.), Deformation Mechanisms, Rheology and Tectonics: From Minerals to the Lithosphere, pp. 159–174.
Rogers, R.D., Karason, H., van der Hilst, R.D., 2002. Epeirogenic uplift above a detached slab in northern Central America. Geology 30 (11), 1031–1034.
Royden, L.H., 1993. Evolution of retreating subduction boundaries formed during continental collision. Tectonics 12 (3), 629–638.
Schmeling, H., Babeyko, A.Y., Enns, A., Faccenna, C., Funiciello, F., Gerya, T., Golabek, G.J., Grigull, S., Kaus, B.J.P., Morra, G., Schmalholz, S.M., van Hunen, J., 2008. A benchmark comparison of spontaneous subduction models—towards a free surface. Phys. Earth Planet. Inter. 171 (1–4), 198–223.
Sengör, A.M.C., Altiner, D., Cin, A., Ustaomer, T., Hsu, K.J., 1988. Origin and assembly of the Tethyside orogenic collage at the expense of Gondwana Land. In: Audley-Charles, M.G., Hallam, A. (Eds.), , pp. 119–181.
Shabanian, E., Bellier, O., Siame, L., Arnaud, N., Abbassi, M.R., Cocheme, J.J., 2009. New tectonic configuration in NE Iran: active strike-slip faulting between the Kopeh Dagh and Binalud mountains. Tectonics 28.
Stein, C.A., Stein, S., 1992. A model for the global variation in oceanic depth and heat flow with lithospheric age. Nature 359, 123–129.
Stern, R.J., 2005. Evidence from ophiolites, blueschists, and ultrahigh-pressure metamorphic terranes that the modern episode of subduction tectonics began in Neoproterozoic time. Geology 33, 557–560.
Turcotte, D.L., Schubert, G., 2002. Geodynamics, Applications of Continuum Physics to Geological Problems, Second Edition. Cambridge University Press.
van de Zedde, D.M.A., Wortel, M.J.R., 2001. Shallow slab detachment as a transient source of heat at midlithospheric depths. Tectonics 20 (6), 868–882.
van den Berg, A.P., van Keken, P.E., Yuen, D.A., 1993. The effects of a composite non-Newtonian and Newtonian rheology on mantle convection. Geophys. J. Int. 115 (1), 62–78.
van der Hilst, R.D., Engdahl, E.R., Spakman, W., Nolet, G., 1991. Tomographic imaging of subducted lithosphere below northwest Pacific island arcs. Nature 353, 37–43.
van der Meulen, M.J., Kouwenhoven, T.J., van der Zwaan, G.J., Meulenkamp, J.E., Wortel, M.J.R., 1999. Late Miocene uplift in the Romagnan Apennines and the detachment of subducted lithosphere. Tectonophysics 315, 315–331.
van Hunen, J., van den Berg, A.P., 2008. Plate tectonics on the early Earth: limitations imposed by strength and buoyancy of subducted lithosphere. Lithos 103 (1–2), 217–235.
van Hunen, J., van den Berg, A.P., Vlaar, N.J., 2002. On the role of subducting oceanic plateaus in the development of shallow flat subduction. Tectonophysics 352, 317–333.
van Hunen, J., Zhong, S., Shapiro, N.M., Ritzwoller, M.H., 2005. New evidence for dislocation creep from 3-D geodynamic modeling of the Pacific upper mantle structure. Earth Planet. Sci. Lett. 238, 146–155.
van Hunen, J., van Keken, P.E., Hynes, A., Davies, G.F., 2008. Tectonics of early Earth: Some geodynamic considerations, in Condie, K.C., and Pease, V., eds., When Did Plate Tectonics Begin on Planet Earth?: Geological Society of America Special Paper 440, p. 157–171. doi: 10.1130/2008.2440(08)
van Keken, P.E., King, S.D., Schmeling, H., Christensen, U.R., Neumeister, D., Doin, M.-P., 1997. A comparison of methods for the modeling of thermochemical convection. J. Geophys. Res. 102, 22477–22495.
Vincent, S.J., Allen, M.B., Ismail-Zadeh, A.D., Flecker, R., Foland, K.A., Simmons, M.D., 2005. Insights from the Talysh of Azerbaijan into the Paleogene evolution of the South Caspian region. Geol. Soc. Am. Bull. 117 (11–12), 1513–1533.
Walker, R.T., Gans, P., Allen, M.B., Jackson, J., Khatib, M., Marsh, N., Zarrinkoub, M., 2009. Late Cenozoic volcanism and rates of active faulting in eastern Iran. Geophys. J. Int. 177 (2), 783–805.
Westaway, R., 1993. Quaternary uplift of southern Italy. J. Geophys. Res. Solid Earth 98 (B12), 21741–21772.
Whalen, J.B., McNicoll, V.J., van Staal, C.R., Lissenberg, C.J., Longstaffe, F.J., Jenner, G.A., van Breeman, O., 2006. Spatial, temporal and geochemical characteristics of Silurian collision-zone magmatism, Newfoundland Appalachians: an example of a rapidly evolving magmatic system related to slab break-off. Lithos 89 (3–4), 377–404.
Wong-A-Ton, S.Y.M., Wortel, M.J.R., 1997. Slab detachment in continental collision zones: an analysis of controlling parameters. Geophys. Res. Lett. 24 (16), 2095–2098.
Wortel, M.J.R., Spakman, W., 1992. Structure and dynamics of subducted lithosphere in the Mediterranean region. Proc. K. Ned. Akad. Wet. 95, 325–347.
Wortel, M.J.R., Spakman, W., 2000. Subduction and slab detachment in the Mediterranean–Carpathian region. Science 290, 1910–1917.
Wortel, R., Govers, R., Spakman, W., 2009. Continental collision and the STEP-wise evolution of convergent plate boundaries: from structure to dynamics. Subduction Zone Geodynamics 47–59.
Yoshioka, S., Wortel, M.J.R., 1995. Three-dimensional numerical modeling of detachment of subducted lithosphere. J. Geophys. Res. 100 (20), 223.
Zhong, S., Zuber, M.T., Moresi, L.N., Gurnis, M., 2000. The role of temperature dependent viscosity and surface plates in spherical shell models of mantle convection. J Geophys Res 105, 11,063–11,082.